Supplement of Atmos. Chem. Phys., 25, 13123–13140, 2025 https://doi.org/10.5194/acp-25-13123-2025-supplement © Author(s) 2025. CC BY 4.0 License.





Supplement of

Simulated mixing in the UTLS by small-scale turbulence using multi-scale chemistry-climate model MECO(n)

Chun Hang Chau et al.

Correspondence to: Chun Hang Chau (cchau@uni-mainz.de) and Holger Tost (tosth@uni-mainz.de)

The copyright of individual parts of the supplement might differ from the article licence.

This supplement presents the evaluation of the newly introduced enhanced vertical grid EH-84 and discusses whether EH-84 performs comparably well to EX-60. In order to evaluate EH-84, we validate the CM10 output from EH-84 with ERA-5 reanalysis data (Hersbach et al., 2020) and also intercompare the EH-84 CM10 output with EX-60. In addition, we performed a sensitivity test of the model TKE on both horizontal and vertical resolution.

5 S1 Basic meteorology

S1.1 Comparison with ERA-5

In this section, the temperature and specific humidity of the CM10 output from EH-84 are compared with the ERA-5 reanalysis data. Since the model outputs from COSMO are height-based and the ERA-5 data are pressure-based, the COSMO output is interpolated to the corresponding pressure level that matches with the ERA-5 data (i.e. 100 hPa, 125 hPa, 150 hPa, 200 hPa, 225 hPa, 250 hPa, 300 hPa, 350 hPa, 400 hPa, 450 hPa and 500 hPa). Figure 1 shows the temperature of the selected pressure levels from COSMO, ERA-5 and the difference (COSMO- ERA-5) for 1st Feb 2016 which is the first day of the simulation. The model results generally agree with the reanalysis data, the patterns of the temperature distribution are generally reproduced in different pressure levels. Although there are some discrepancies between COSMO and ERA5, they are most likely because of the slightly shifted distribution of temperature, the general patterns with the cooler and warmer air mass are able to reproduce distinctly. Figure 2 shows the same plots as Figure S1 but for the last day of the simulation (7th Feb 2016). The model results are still able to reproduce a similar pattern compared to the ERA-5 data. However, the COSMO temperature is generally cooler than the reanalysis data, there is a systematic cold bias for the whole domain with at most more than 4 k cooler. Figure S3 shows the specific humidity of the selected pressure levels for 1st Feb 2016. It can be seen that there is a generally good agreement between the COSMO and ERA-5 data for most of the pressure levels except for the 100 hPa where COSMO is significantly drier than ERA-5. Figure S4 shows the specific humidity for 7th Feb 2016. The specific humidity was still able to produce similar patterns below 200 hPa. For the higher levels, the distribution starts to vary from the ERA-5 data, but most of them remain in the same order of magnitude. Considering the large uncertainty for the UTLS water vapour in reanalysis data (Fujiwara et al., 2022), the variation of the specific humidity is still within an acceptable margin.

S1.2 Discussion on the cold bias

In order to investigate whether the discrepancy (especially the cold bias) between the model and ERA-5 data corresponds to the enhancing vertical resolution, the EH-84 output is further compared with the tested EX-60 output. The model setup for EX-60 is mostly consistent with the setup of EH-84 except for the vertical grid in order to investigate the effect of increasing vertical resolution in EH-84. Both temperature and specific humidity show good agreement with only some slight differences in the order of magnitudes (Figure S5, S6). To elucidate what is responsible for the cold bias, we then compared both the ERA-Interim reanalysis data which initialized the simulation, the EMAC and CM40 output with ERA-5 data. Figure S7 shows the temperature for the last day, ERA-I has no distinct difference when compared with the ERA-5 data. However, the EMAC and CM40 output show a similar cold bias as the CM10 output, which suggests that the cold bias from CM10 originates from EMAC rather than the COSMO model dynamics or the enhanced vertical grid of COSMO.

S1.3 Conclusion

To conclude, the enhanced vertical grid EH-84 for COSMO is able to simulate the atmosphere reasonably. Although there is some discrepancy, the temperature pattern from ERA-5 is generally well produced by the model as well as the relative humidity. The systematic cold bias that occurs in EH-84 is also found in EX-60, indicating that the occurrence of the cold bias is not a result of the constantly increased vertical resolution in the UTLS. Considering the strong alignment between the EH-84 and EX-60 output and the latter is well-tested and well-matched with the observation. The model output from the enhanced vertical grid EH-84 can be seen as reliable and suitable to the needs of this study.

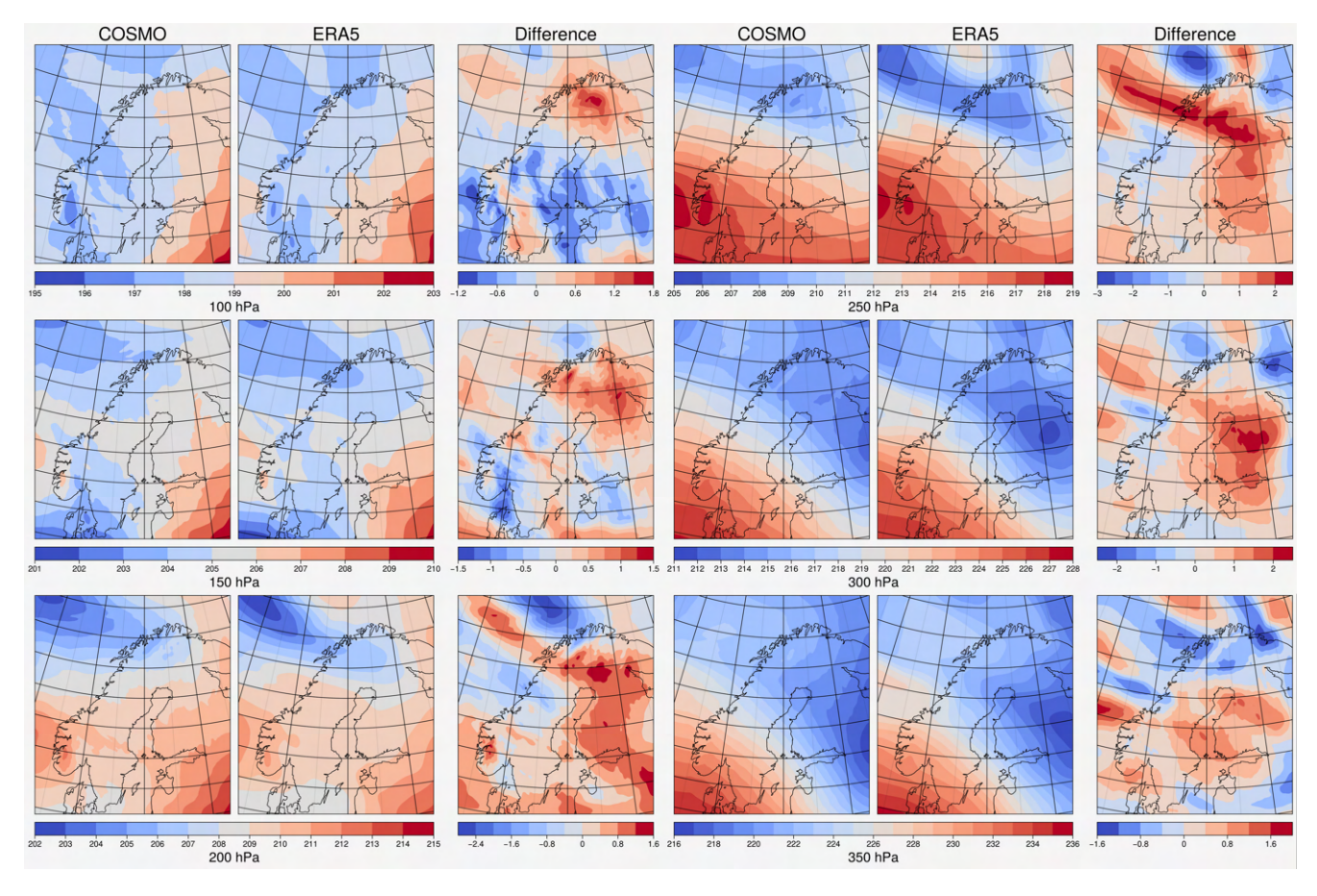


Figure S1. Daily average temperature(K) of 100, 150, 200, 250, 300, 350 hPa at 2016-02-01 for COSMO, ERA5 and the difference.

S2 Sensitivity test

We performed sensitivity tests of the model TKE on both the horizontal and vertical resolution. Results show that TKE is sensitive to the vertical resolution but not the horizontal resolution. The occurrence of high TKE values is more frequent in EH84 than in EX60 (figure S9). The higher vertical resolution results in a more frequent high TKE occurrence. However the occurrence of high TKE values in CM10 and CM40 have no distinct difference as discovered in EH84 and EX60 (figure S10), the finer horizontal resolution does not result in a significant change on TKE. We further investigate the sensitivity of mixing on different resolutions. The EH84 setup results in significantly stronger mixing than EX60 (figure S11) which is as expected considering TKE is a crucial parameter in the turbulence scheme in COSMO. However, the mixing in CM10 is also significantly stronger than in CM40 (figure S12) even though there is no significant difference in TKE, such differences could be attributed to the finer horizontal resolution providing a more detail tropopause which creates a stronger gradient that strengthens the mixing.

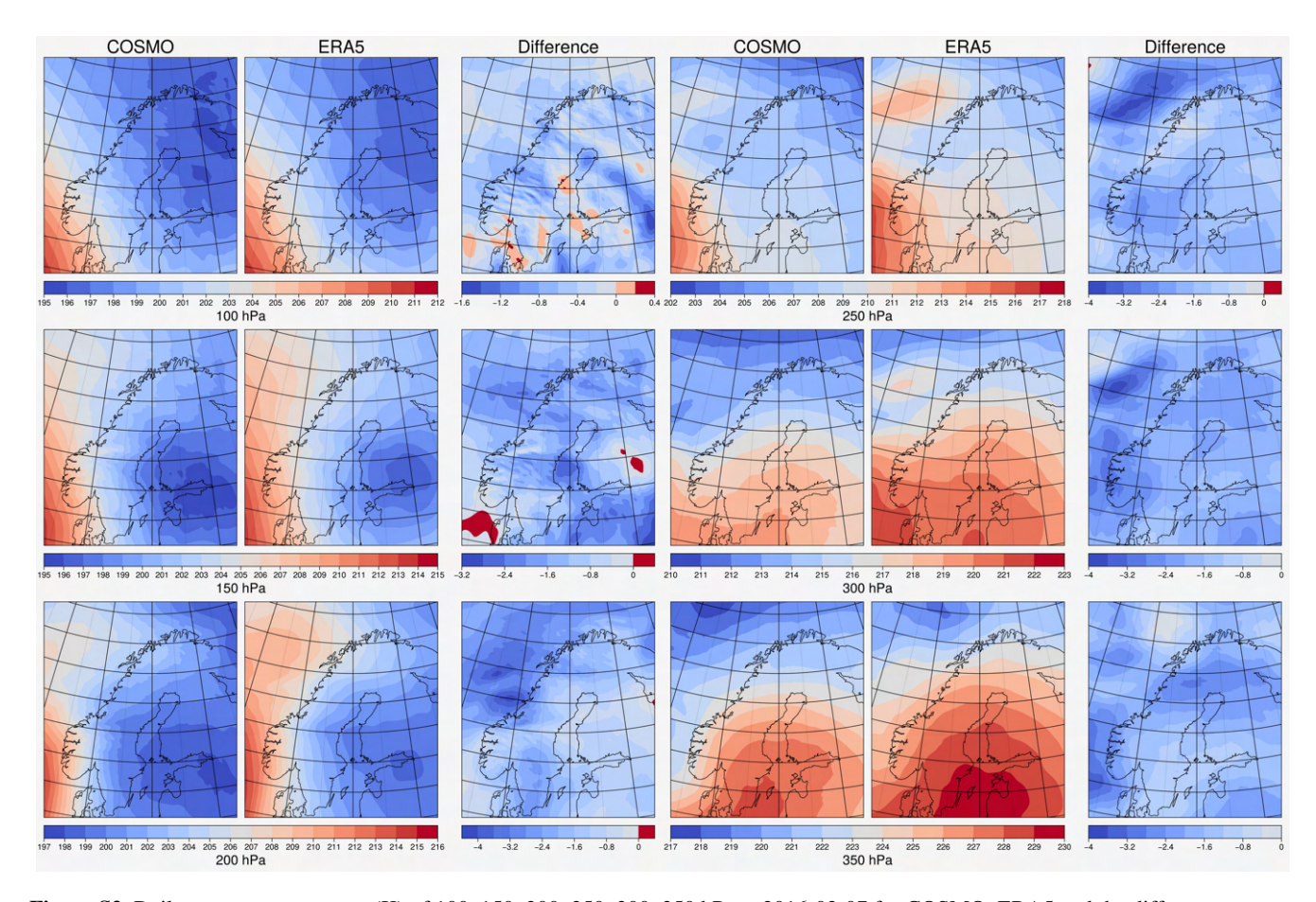


Figure S2. Daily average temperature(K) of 100, 150, 200, 250, 300, 350 hPa at 2016-02-07 for COSMO, ERA5 and the difference.

References

55

Fujiwara, M., Manney, G., Gray, L., and Wright, J.: SPARC Report No. 10, WCRP Report 6/2021, 2022.

Hersbach, H., Bell, B., Berrisford, P., Hirahara, S., Horányi, A., Muñoz-Sabater, J., Nicolas, J., Peubey, C., Radu, R., Schepers, D., Simmons, A., Soci, C., Abdalla, S., Abellan, X., Balsamo, G., Bechtold, P., Biavati, G., Bidlot, J., Bonavita, M., De Chiara, G., Dahlgren, P., Dee, D., Diamantakis, M., Dragani, R., Flemming, J., Forbes, R., Fuentes, M., Geer, A., Haimberger, L., Healy, S., Hogan, R. J., Hólm, E., Janisková, M., Keeley, S., Laloyaux, P., Lopez, P., Lupu, C., Radnoti, G., de Rosnay, P., Rozum, I., Vamborg, F., Villaume, S., and Thépaut, J.-N.: The ERA5 global reanalysis, Quarterly Journal of the Royal Meteorological Society, 146, 1999–2049, https://doi.org/10.1002/qi.3803, 2020.

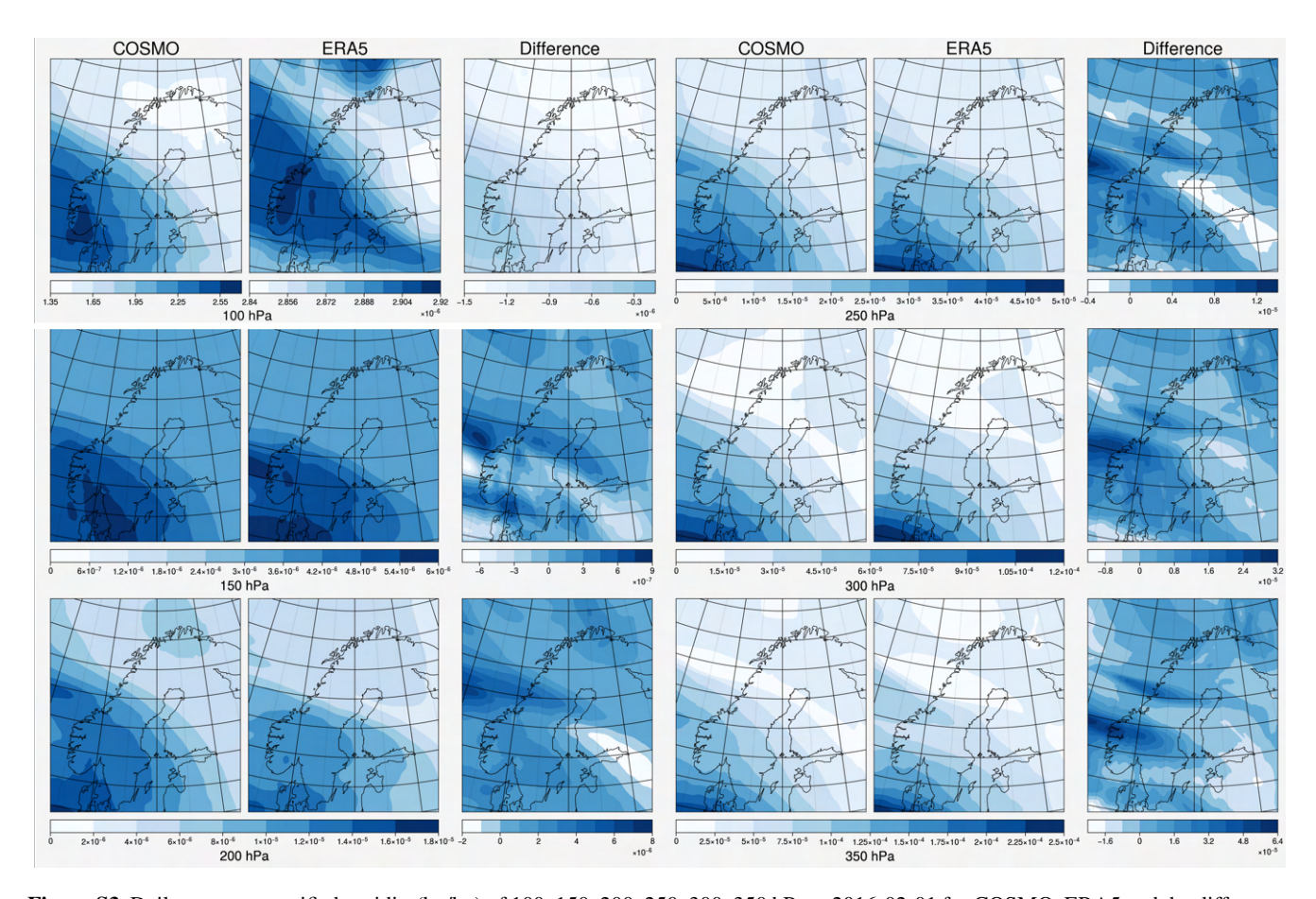


Figure S3. Daily average specific humidity(kg/kg) of 100, 150, 200, 250, 300, 350 hPa at 2016-02-01 for COSMO, ERA5 and the difference.

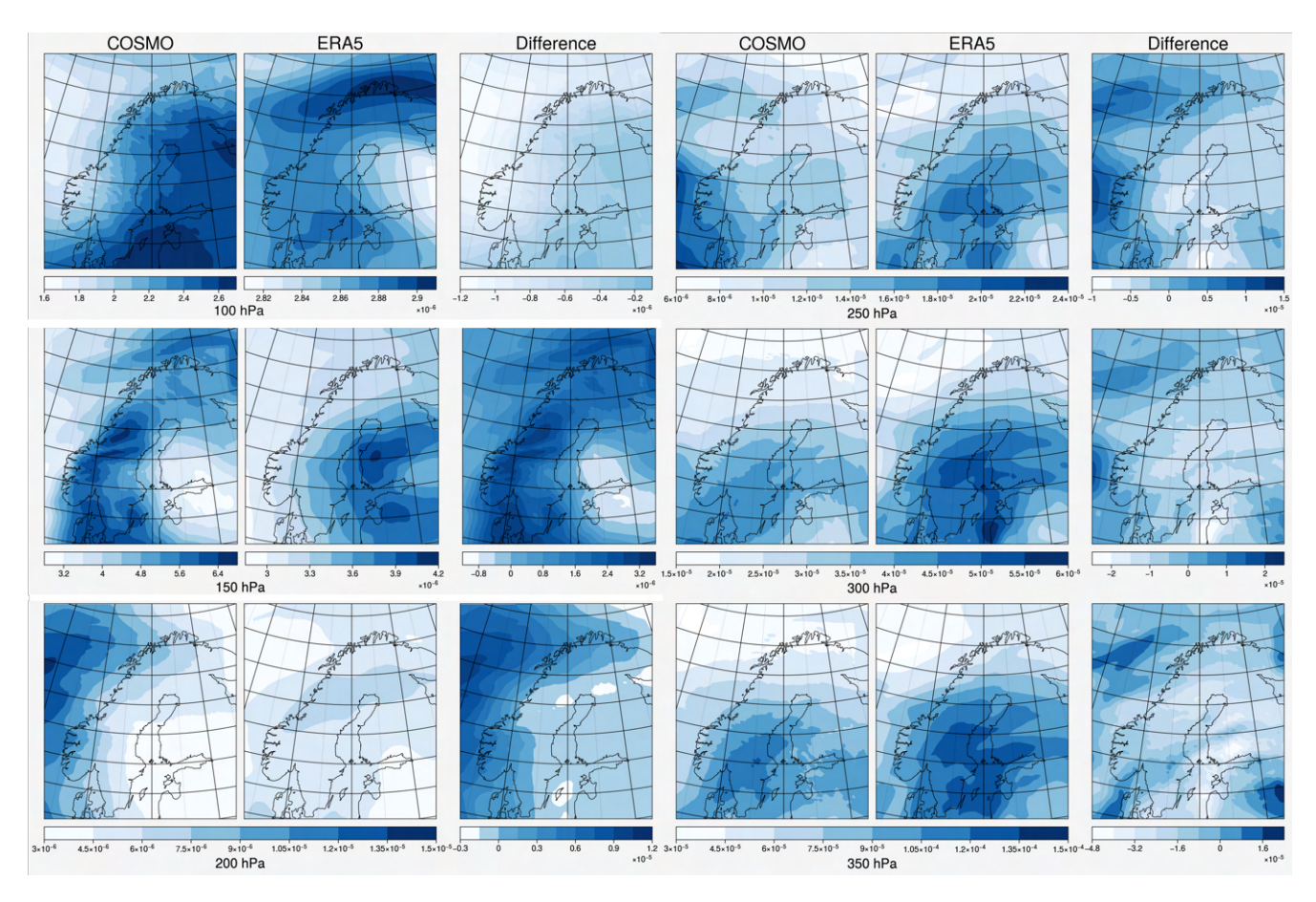


Figure S4. Daily average specific humidity(kg/kg) of 100, 150, 200, 250, 300, 350 hPa at 2016-02-07 for COSMO, ERA5 and the difference.

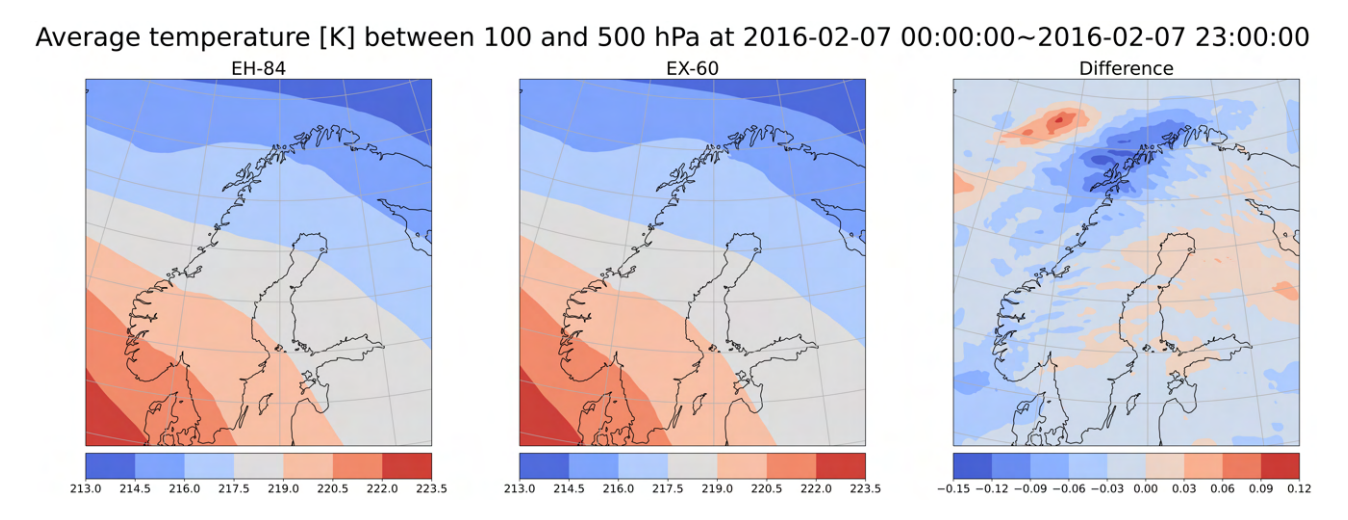
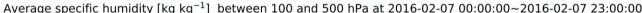


Figure S5. Daily average temperature between 100 and 500 hPa at 2016-02-07 for EH-84 (left), EX-60 (middle) and the difference (right).



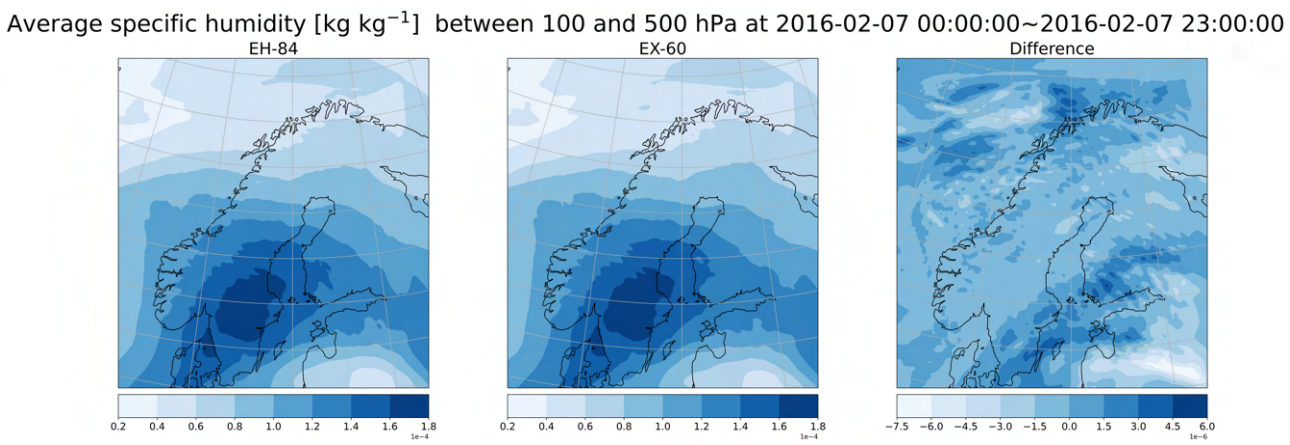


Figure S6. The daily average specific humidity between 100 and 500 hPa at 2016-02-07 for EH-84 (left), EX-60 (middle) and the difference (right).

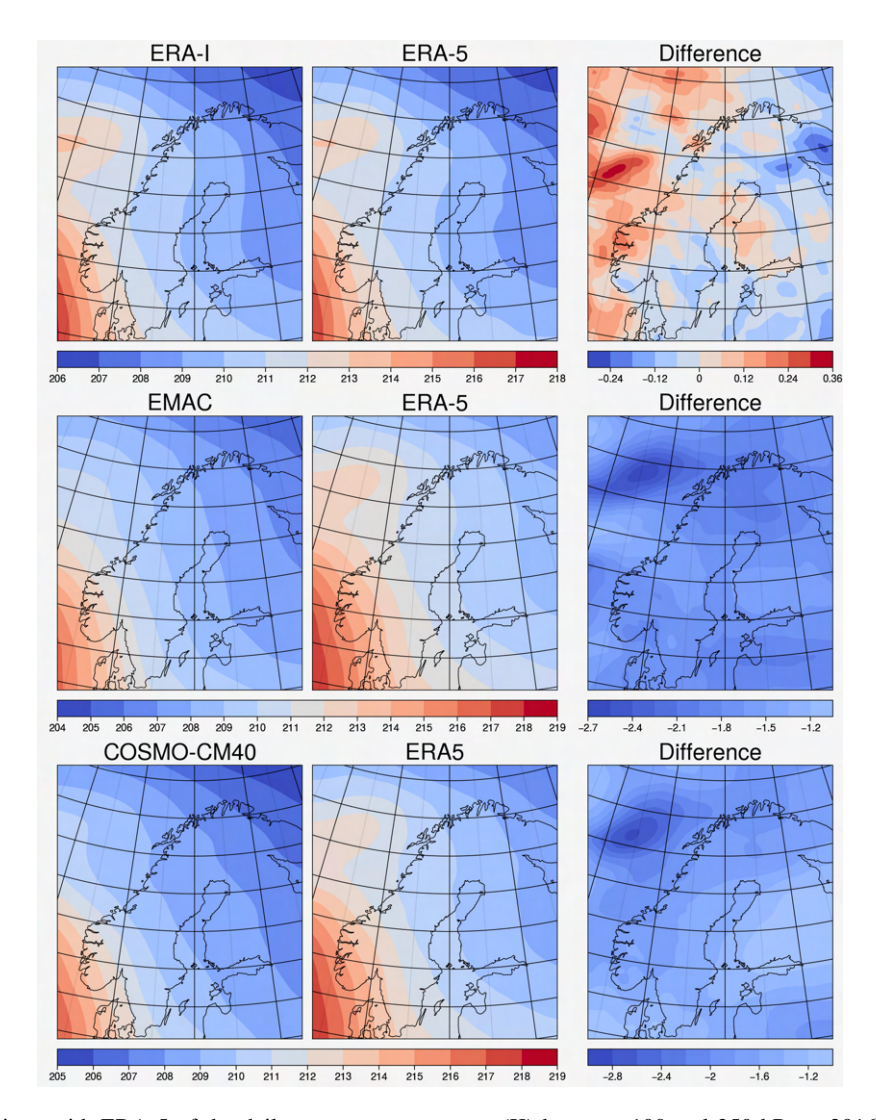


Figure S7. The comparison with ERA-5 of the daily average temperature (K) between 100 and 350 hPa at 2016-02-07 for ERA-I (top), EMAC (middle) and COSMO-CM40 (bottom).

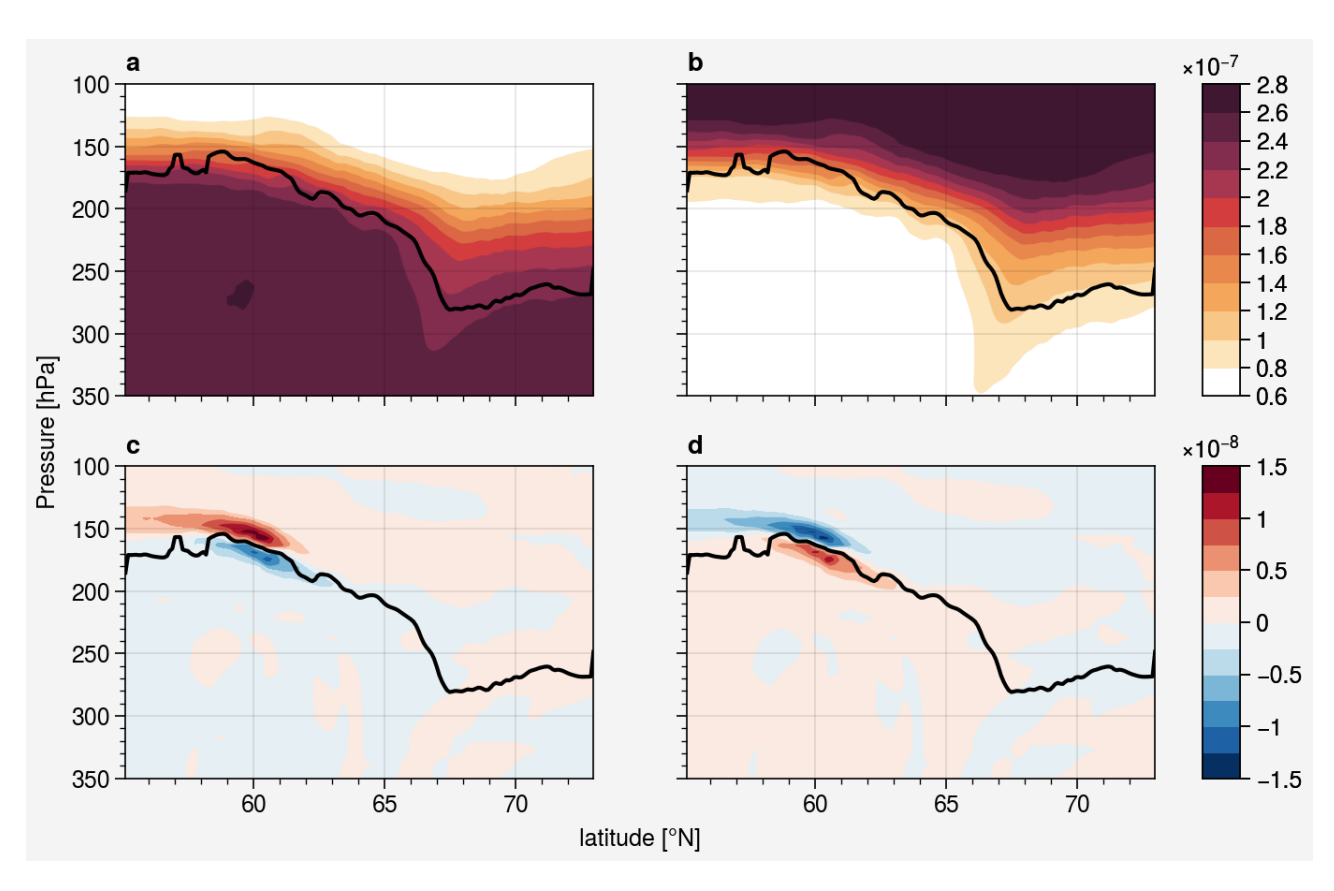


Figure S8. Cross section of distribution (a) N2O-like tracers (mol/mol), (b) Inverted N2O-like tracers (mol/mol); difference (vdiff on - off) (c) N2O-like tracers (mol/mol), (d)Inverted N2O-like tracers (mol/mol) at 2016-02-05 18:00.

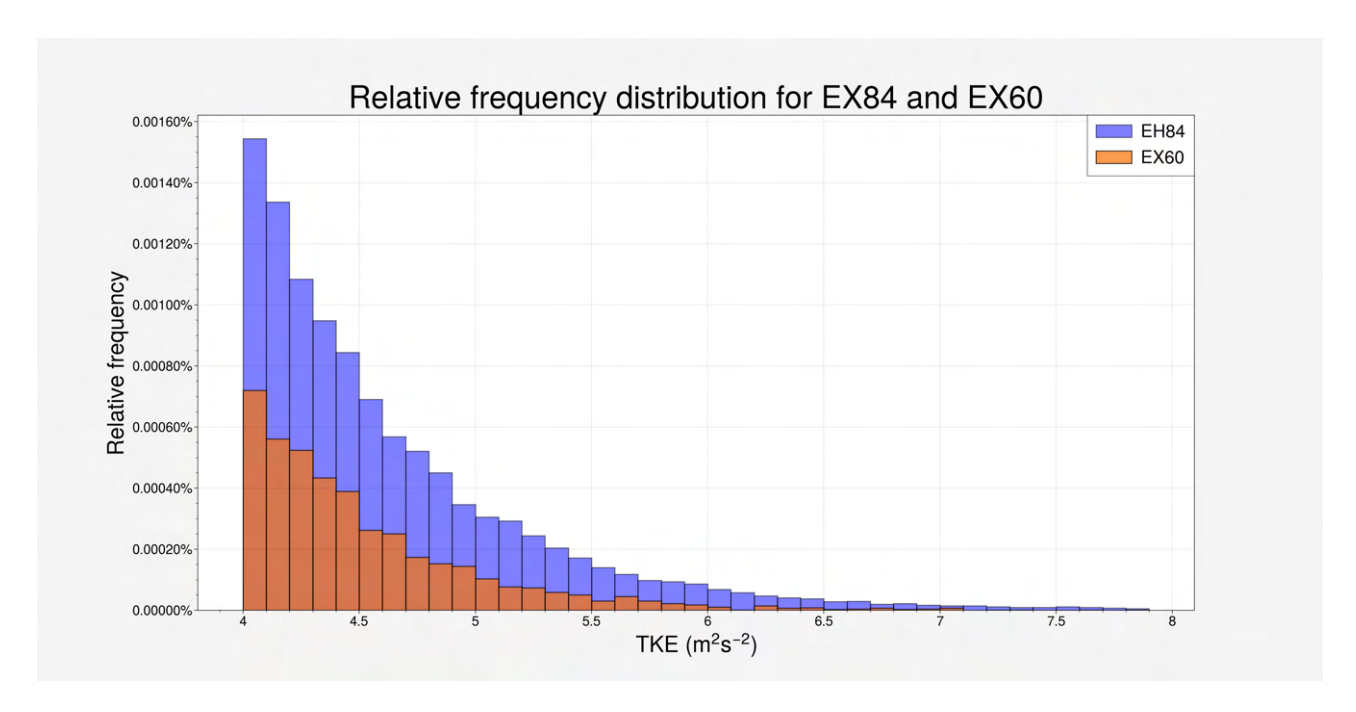


Figure S9. Relative frequency distribution of high TKE value for EH84 (blue) and EX60 (orange)

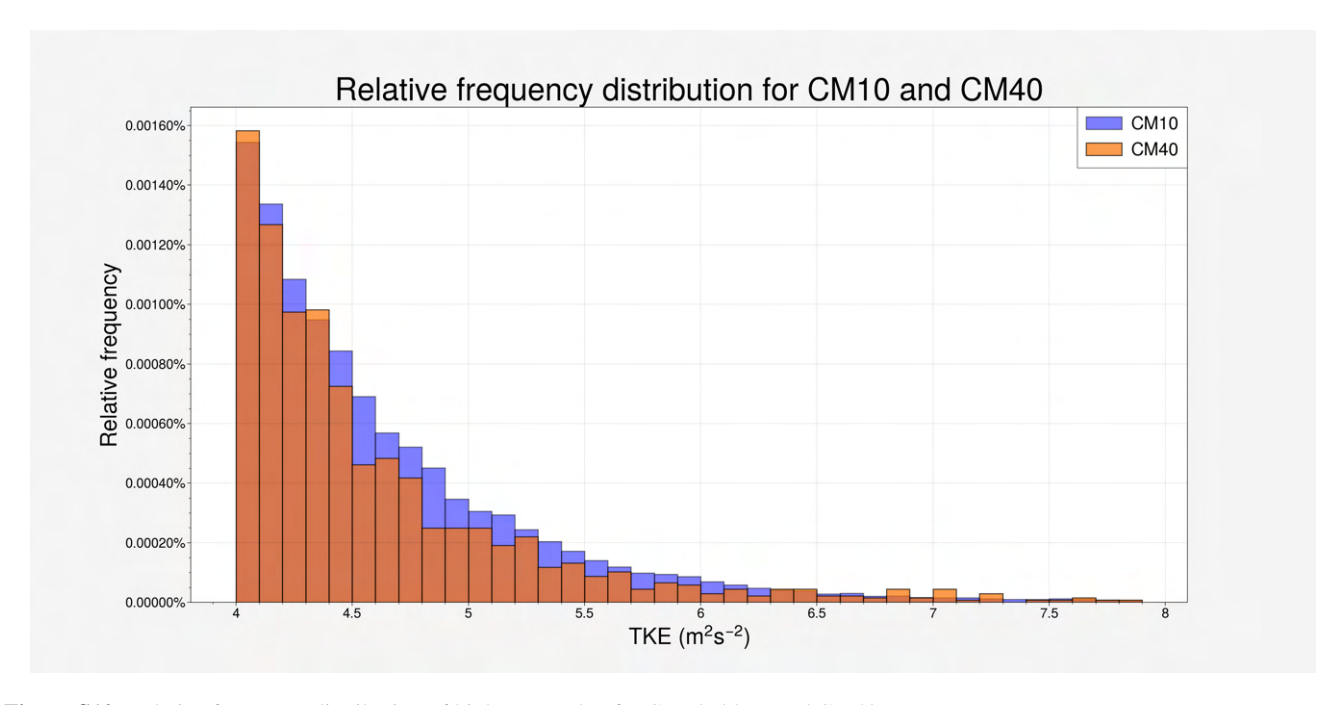


Figure S10. Relative frequency distribution of high TKE value for CM10 (blue) and CM40 (orange).

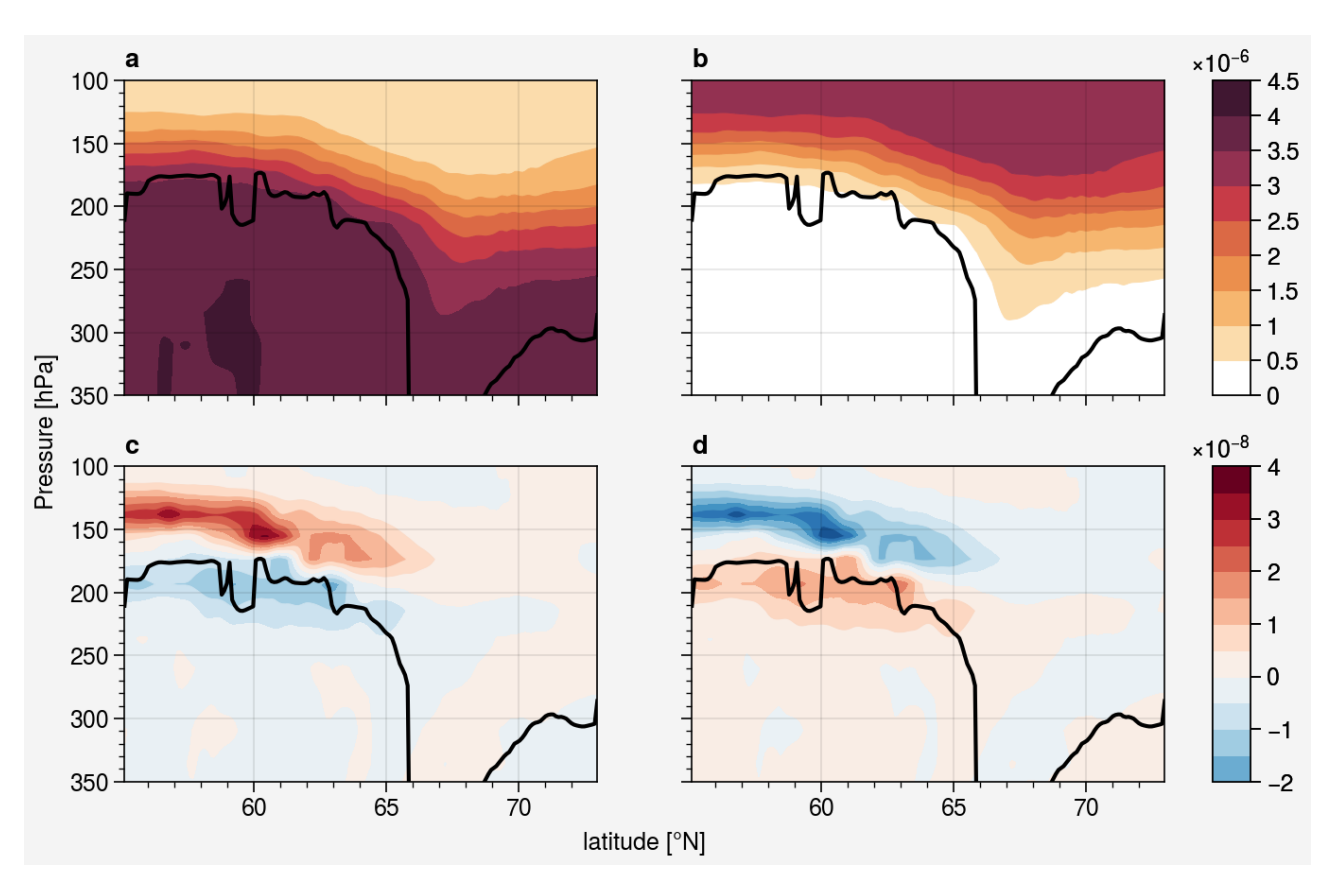


Figure S11. Cross section of distribution for EX60 (a) Inverted O3-like tracers (mol/mol), (b) O3-like tracers (mol/mol); the difference (vdiff on - off) (c) Inverted O3-like tracers (mol/mol), (d)O3-like tracers (mol/mol) at 2016-02-05 18:00.

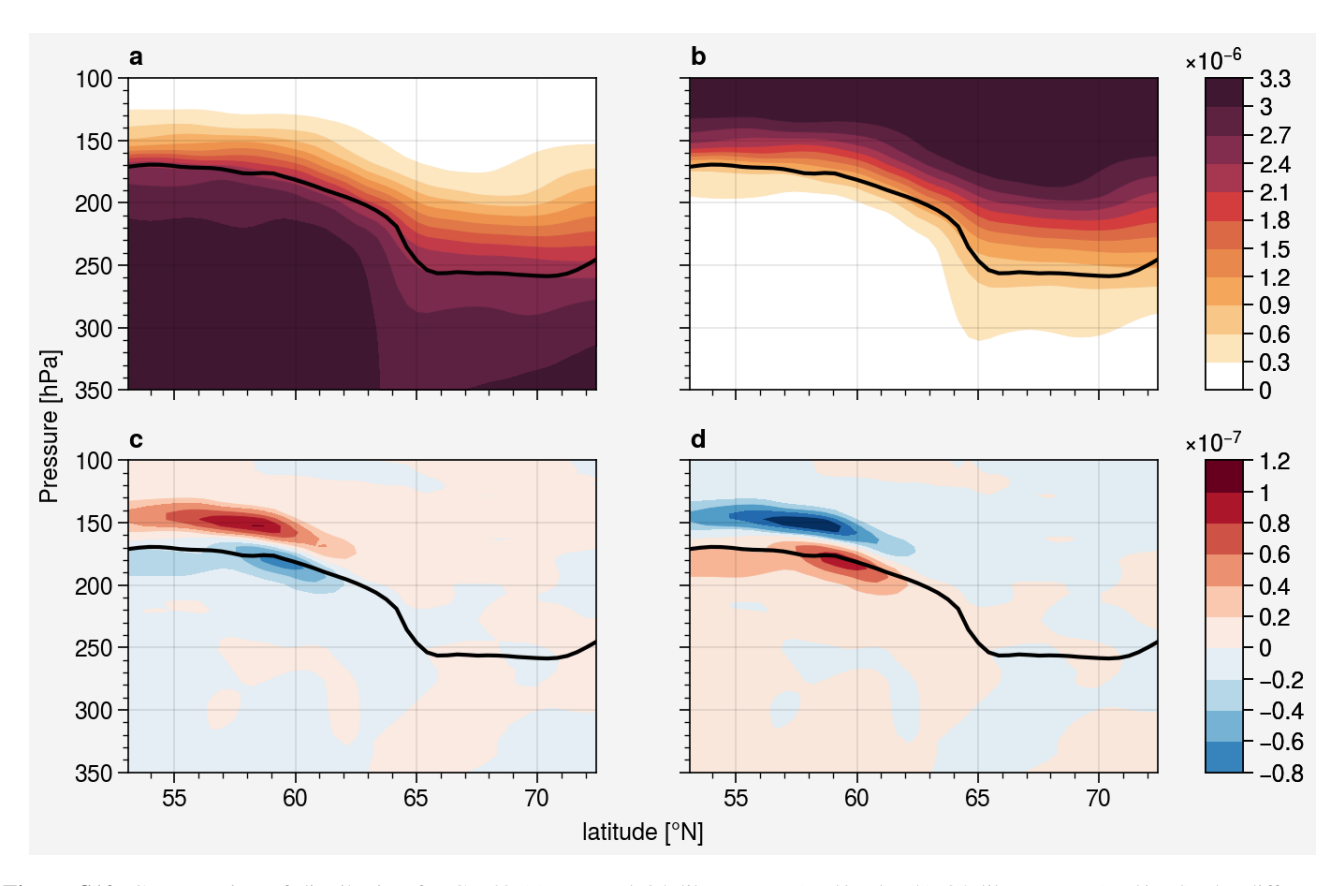


Figure S12. Cross section of distribution for CM40 (a) Inverted O3-like tracers (mol/mol), (b) O3-like tracers (mol/mol); the difference (vdiff on - off) (c) Inverted O3-like tracers (mol/mol), (d)O3-like tracers (mol/mol) at 2016-02-05 18:00.

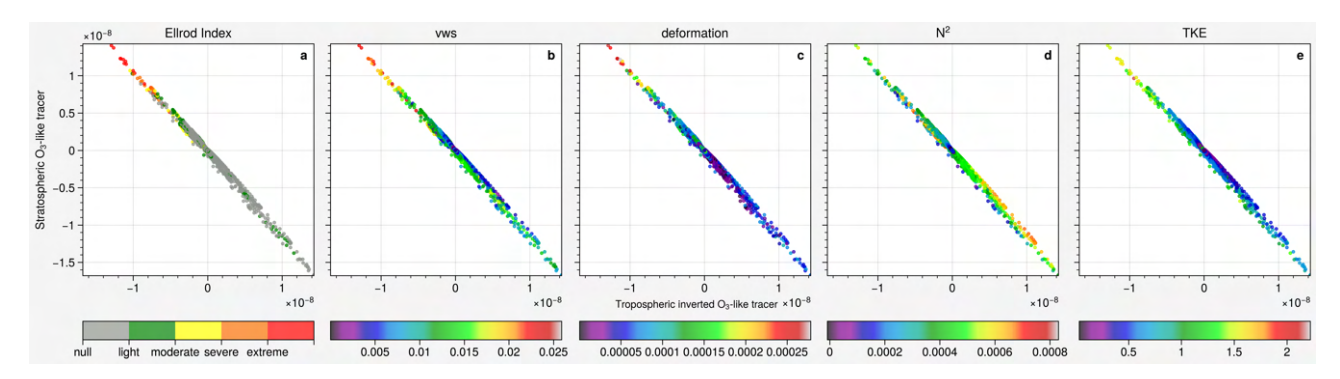


Figure S13. Delta tracer-tracer correlation of stratospheric inverted N2O-like/tropospheric N2O-like tracers (mol/mol) color-coded with (a) Ellrod Index(s^{-2}), (b) vertical wind shear (s^{-1}), (c) deformation (s^{-1}), (d) Brunt–Väisälä frequency (s^{-2}) and (e) turbulence kinetic energy ($m^2 \, s^{-2}$) at 2016-02-05 18:00.

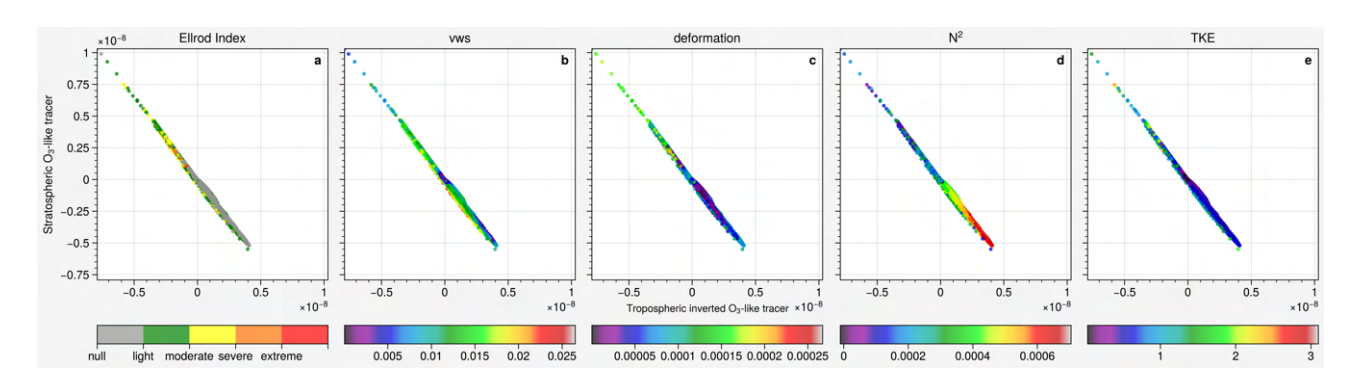


Figure S14. Delta tracer-tracer correlation of stratospheric inverted N2O-like/tropospheric N2O-like tracers (mol/mol) color-coded with (a) Ellrod Index(s^{-2}), (b) vertical wind shear (s^{-1}), (c) deformation (s^{-1}), (d) Brunt–Väisälä frequency (s^{-2}) and (e) turbulence kinetic energy ($m^2 \, s^{-2}$) at 2016-02-05 05:00.

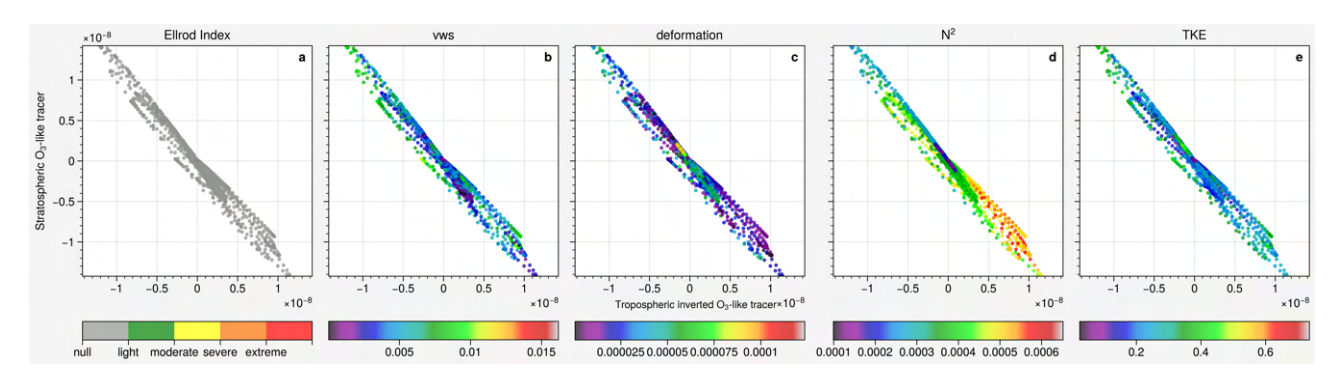


Figure S15. Delta tracer-tracer correlation of stratospheric inverted N2O-like/tropospheric N2O-like tracers (mol/mol) color-coded with (a) Ellrod Index(s^{-2}), (b) vertical wind shear (s^{-1}), (c) deformation (s^{-1}), (d) Brunt–Väisälä frequency (s^{-2}) and (e) turbulence kinetic energy ($m^2 \, s^{-2}$) at 2016-02-03 22:00.

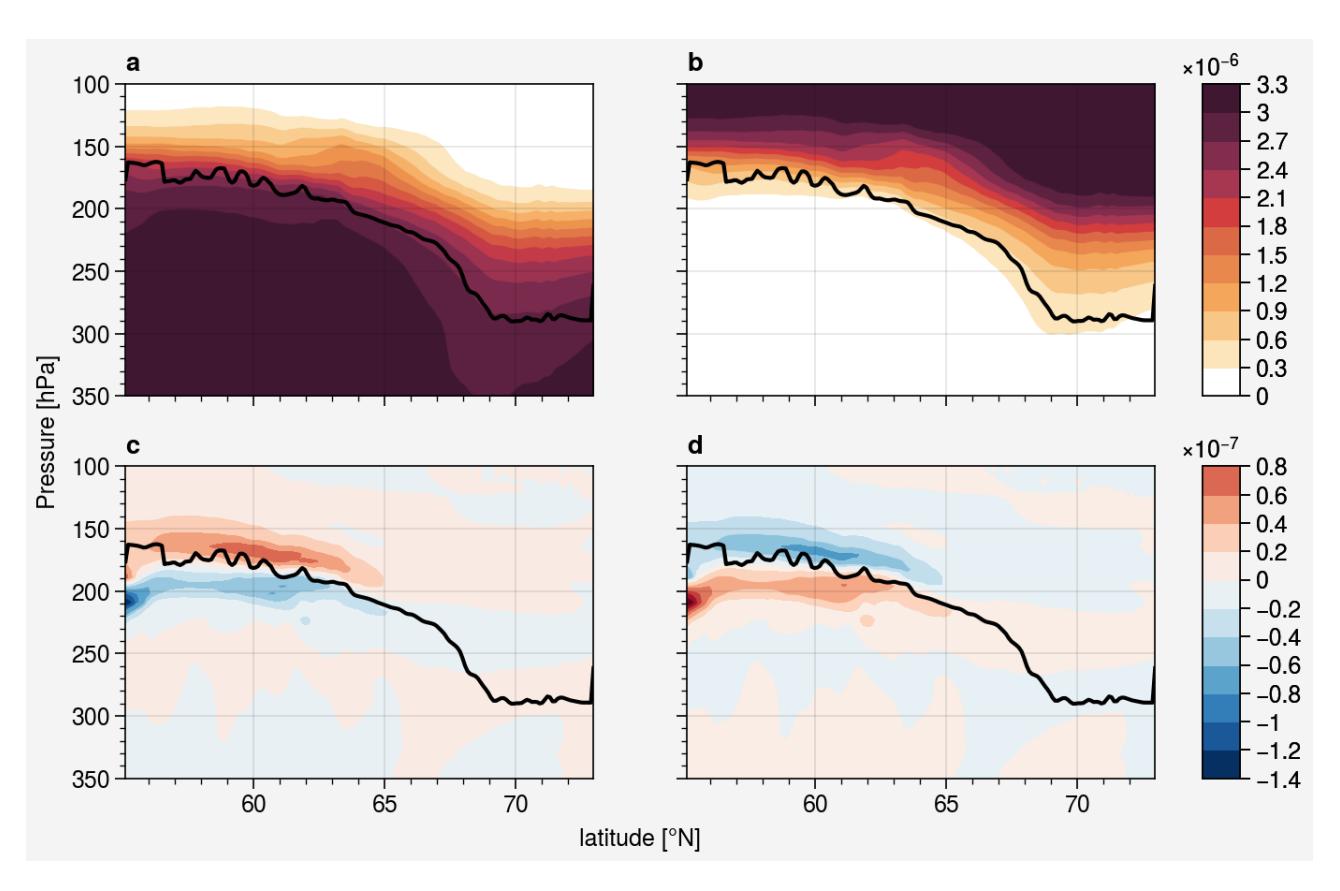


Figure S16. Cross section of distribution for Case 2 (a) Inverted O3-like tracers (mol/mol), (b) O3-like tracers (mol/mol); the difference (vdiff on - off) (c) Inverted O3-like tracers (mol/mol), (d)O3-like tracers (mol/mol).

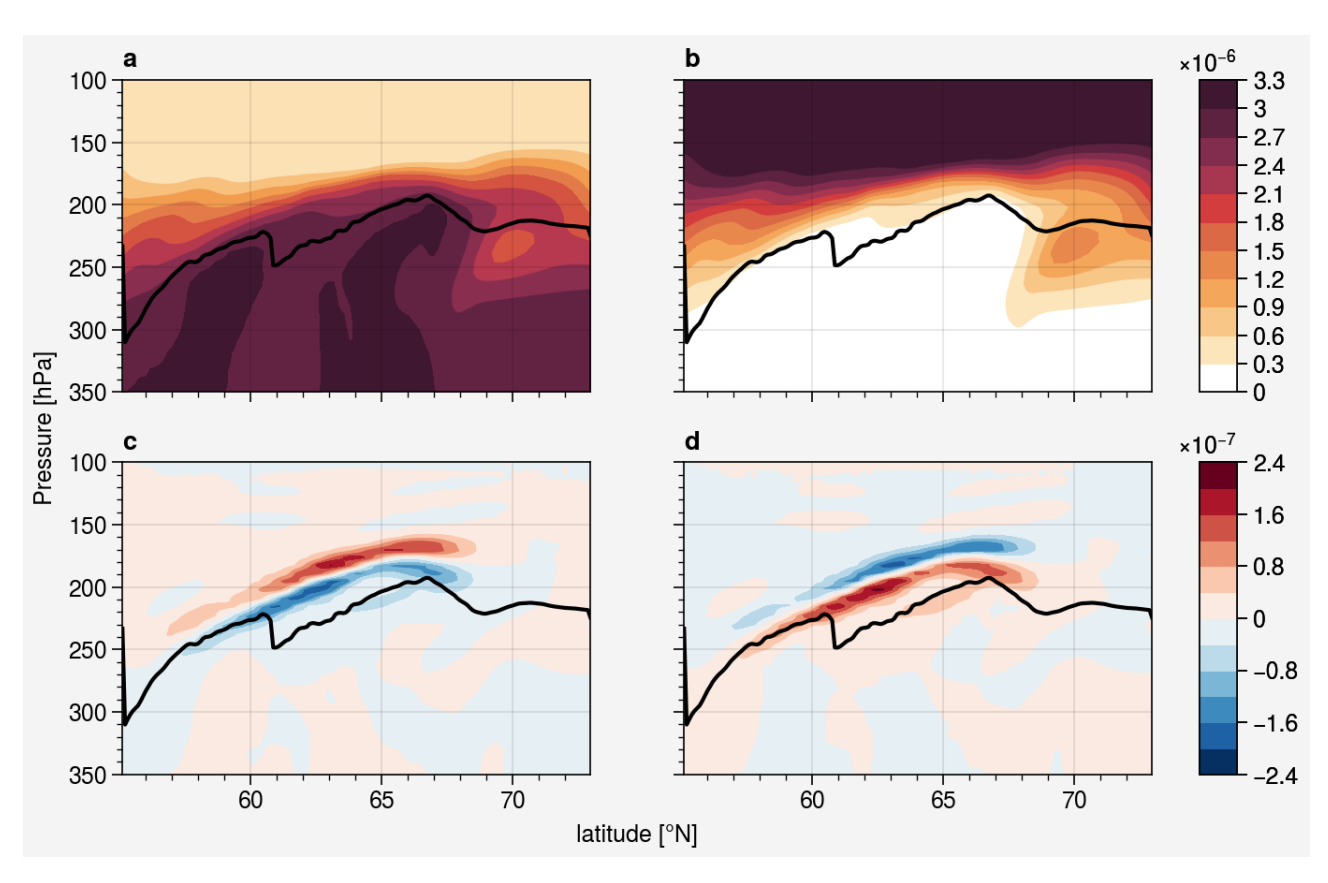


Figure S17. Cross section of distribution for Case 3 (a) Inverted O3-like tracers (mol/mol), (b) O3-like tracers (mol/mol); the difference (vdiff on - off) (c) Inverted O3-like tracers (mol/mol), (d)O3-like tracers (mol/mol).

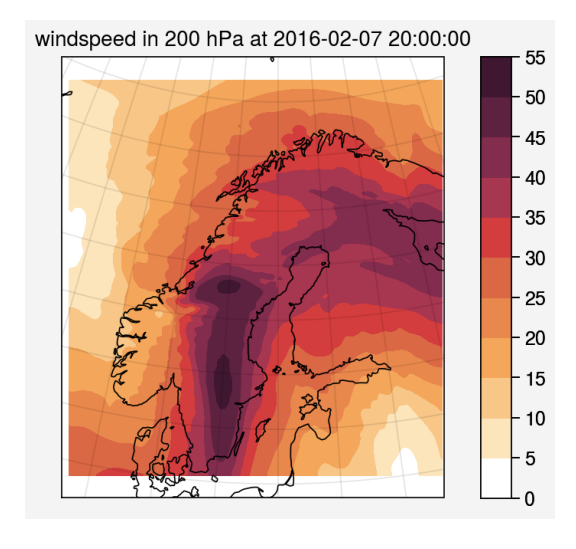


Figure S18. Horizontal wind speed (m/s) at 200 hPa at 2016-02-07 20:00 for CM10.

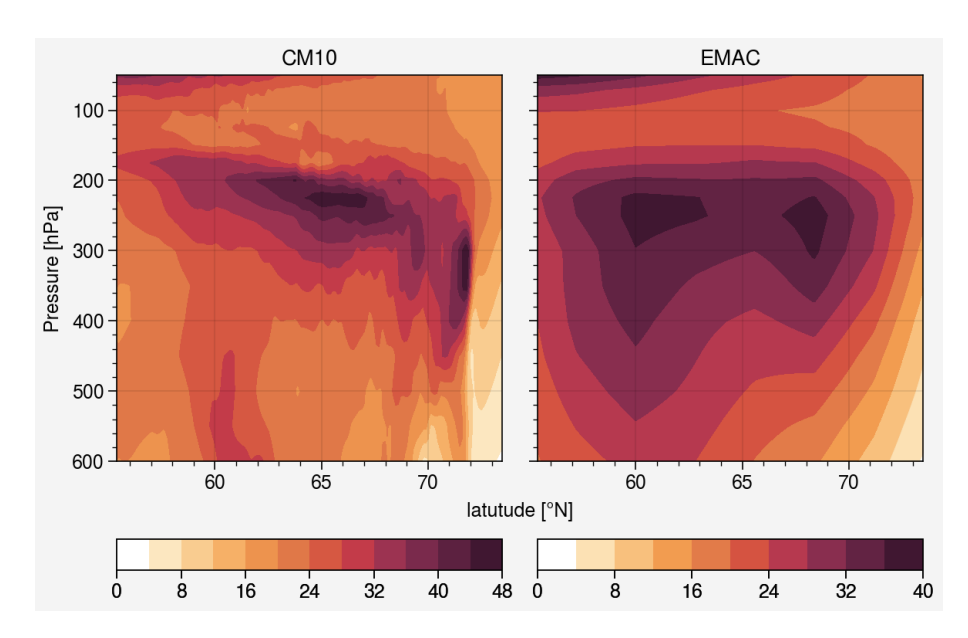


Figure S19. Cross section of horizontal wind (m/s) at 2016-02-07 20:00 for (a) CM10, (b) EMAC

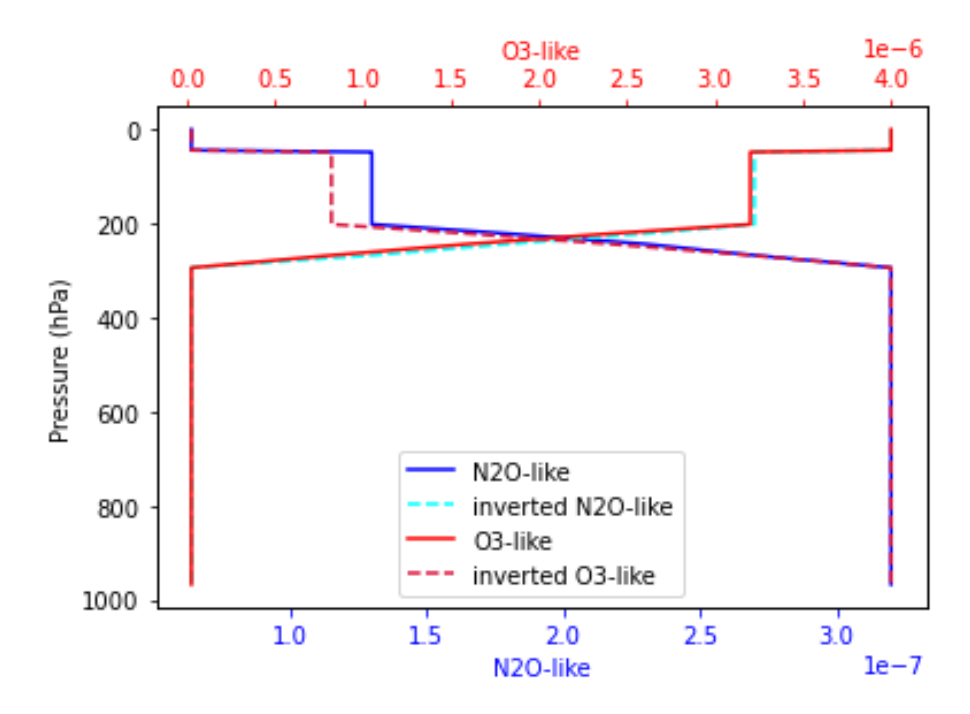


Figure S20. Vertical profile of the tracer N2O-like (mol/mol), inverted N2O-like (mol/mol), O3-like (mol/mol) and inverted O3-like tracer (mol/mol).

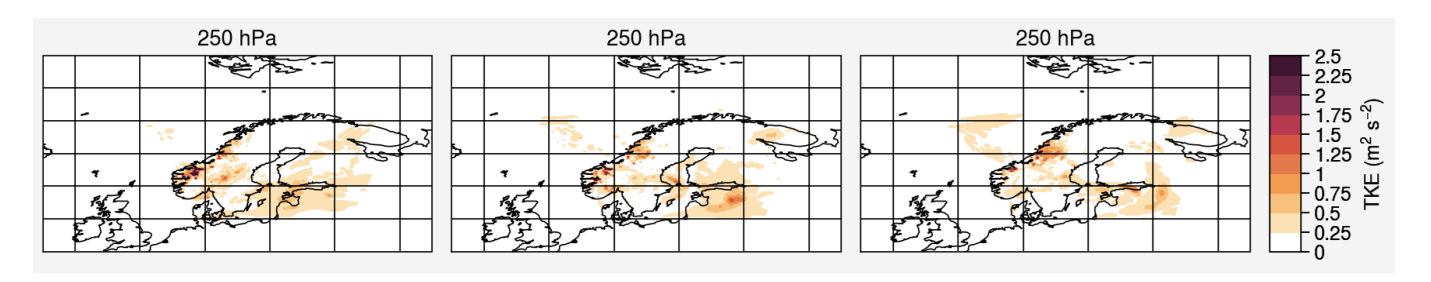


Figure S21. Modeled TKE at 250 hPa for CM10 at 2016-02-03 11:00(left), 18:00 (middle) and 22:00 (right).

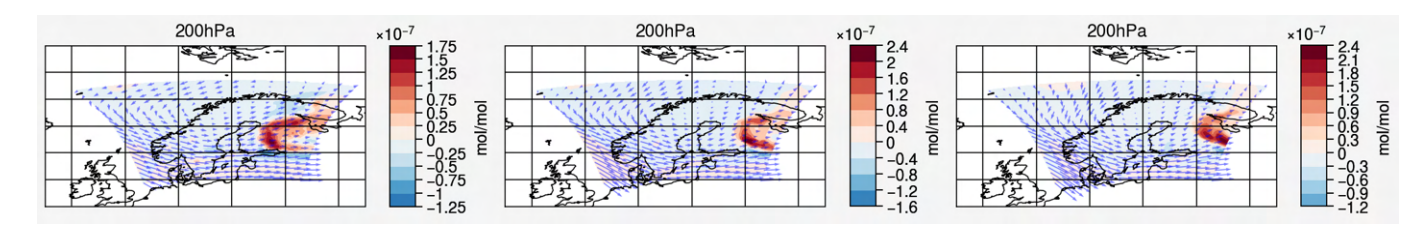


Figure S22. O3-like tracers difference(vdiff on - off) at 200 hPa at 2016-02-03 11:00(left), 18:00 (middle) and 22:00 (right), the blue arrow indicates the wind direction and wind speed.